Katarzyna Staszak[1]

Membrane processes

[1] Institute of Chemical Technology & Engineering, Poznan University of Technology, Berdychowo 4, 60-965 Poznań, Poland, E-mail: katarzyna.staszak@put.poznan.pl

Abstract:
The membrane processes have played important role in the industrial separation process. These technologies can be found in all industrial areas such as food, beverages, metallurgy, pulp and paper, textile, pharmaceutical, automotive, biotechnology and chemical industry, as well as in water treatment for domestic and industrial application. Although these processes are known since twentieth century, there are still many studies that focus on the testing of new membranes' materials and determining of conditions for optimal selectivity, i. e. the optimum transmembrane pressure (TMP) or permeate flux to minimize fouling. Moreover the researchers proposed some calculation methods to predict the membrane processes properties. In this article, the laboratory scale experiments of membrane separation techniques, as well their validation by calculation methods are presented. Because membrane is the "heart" of the process, experimental and computational methods for its characterization are also described.

Keywords: membrane process, modeling, fouling, retention
DOI: 10.1515/psr-2017-0142

1 Basic principle of membrane process

The performance or efficiency of a given membrane is determined by two parameters – its selectivity and the flow through the membrane. The latter, often denoted as the flux (J) or permeation rate, is defined as the volume flowing ($\dot{V}$) through the membrane per unit area (A) and time (t):

$$J = \frac{\dot{V}}{A \times t} \tag{1}$$

The selectivity of a membrane is generally expressed by one of two parameters – the retention (R) or the separation factor (α). For dilute aqueous mixtures, consisting of a solvent (mostly water) and a soluble, it is more convenient to express the selectivity in terms of the retention towards the solute. The solute is partly or completely retained while solvent molecules pass freely through the membrane. The retention is given by equation:

$$R = \frac{c_f - c_p}{c_f} = 1 - \frac{c_p}{c_f} \tag{2}$$

where c_f is the concentration in the feed, c_p – concentration in the permeate.

The separation factor generally is used for gas or organic liquids mixtures and it is expressed as:

$$\alpha_{A/B} = \frac{\frac{y_A}{y_B}}{\frac{x_A}{x_B}} \tag{3}$$

where y is the concentration in the permeate, x – concentration in the feed.

1.1 Retention

Mostly in the mathematical description and modeling of membrane processes permeate fluxes are taken into account. Because in the process of membrane filtration the flux usually changes over time due to fouling, so its

Katarzyna Staszak is the corresponding author.

modeling is described in detail in Section 1.2. Much less work can be found on retention modeling. It is not possible to talk about a generalized retention model because of the fact that, depending on the membrane process considered, there are different mechanisms of separation. The membrane separation methods can be divided into classes according to their separation characteristics: (i) separation by sieving action, in porous membranes; (ii) separation due to a difference in affinity and diffusivity, in dense membranes; (iii) separation due to a difference in charge of molecules, in charged membranes; (iv) carrier-facilitated transport; (v) the process of time-controlled release by diffusion [1]. Therefore, only the selected modeling methods of membrane filtration are presented below. An interesting example is nanofiltration. It is a separation technique where selectivity is governed by size selectivity, electrical surface charge and diffusion mechanisms. Thus some interactions that affect rejection as steric hindrance effects (sieving effect), Donnan exclusion and electrostatic repulsion (charge effect) and hydrophobic–adsorptive interaction should be considered in this process [2].

Moreover, very important aspect in the modeling is the characterization of physicochemical properties of compounds and characterization of the membrane materials. These properties are helpful in understanding the transport and retention of compounds during the membrane process.

In the nanofiltration process the charged and uncharged compounds can be rejected, thus the models for their retention are divided also for those for charged and uncharged substances. In the literature, several models for maximal retention of uncharged compounds are proposed, i. e. the steric hindrance pore (SHP) model, the model of Zeman and Wales, the log-normal model and an adapted version of the log-normal model [3]. The maximal retention is defined as the calculated retention corresponds to the retention at an infinite pressure. Because pressure dependence of retention is not included in the models, in real systems the retention is lower, due to the contribution of diffusion to the transport process. These models can be used not only in nanofiltration but also in all filtration process where sieving effect of retention is considered, such as microfiltration or ultrafiltration.

Transport of uncharged compounds in nanofiltration is a combination of diffusion (first term in eq. (4)) and convection (second term in eq. (4)). Thus, equation for flux of dissolved component (J_s) is presented as [4, 5]:

$$J_s = -P\Delta x\frac{dc}{dx} \pm (1-\sigma)\, J_v c \tag{4}$$

J_v is the water flux and is equal to:

$$J_v = L_p\ (TMP - \sigma\Delta\pi) \tag{5}$$

Integration of eq. (4), with following boundary conditions [6]: $c_s = c_0$ for $x = 0$ and $c_s = c_p$ for $x = \Delta x$ and using eq. (5) the retention (R) is directly related to volumetric flux and can be calculated as:

$$R = \frac{\sigma\,(1-F)}{1-\sigma F} \tag{6}$$

where

$$F = \exp\left(-\frac{1-\sigma}{P}J_v\right) \tag{7}$$

At higher values of J_v, the exponential term in eq. (7) tends to zero and R will be equal to σ. Thus σ is a reflection coefficient of a given component and means the maximal possible retention for that component.

In eqs (4)–(7) P is a permeability, which described the transport of a molecule by diffusion; $\Delta\pi$ is osmotic pressure difference across the membrane; Δx is the membrane thickness; subscripts 0, p and s in c are concentrations in the feed solution, in the permeate and in the membrane, respectively.

SHP model is the model where the reflection coefficient is calculated from the pore size of the membrane and the diameter of the molecule. In this model there is big simplification that all membrane's pores have the same size [7]. According to the SHP model membrane is represented as a bundle of cylindrical pores, with the same diameter. During the transport of solution through membrane the molecules with bigger or the same size as the pore diameter are completely retained. Moreover, there is a partially retention of molecules with smaller diameter than pore size due to a certain amount of sterical hindrance and interactions with the pore wall. Thus reflection coefficient can be related to the effect of the pore wall (wall correction parameter H_F) and sterical hindrance during transport through the pore (S_F) according to the equation:

$$\sigma = 1 - H_F S_F \tag{8}$$

where

$$H_F = 1 + \frac{16}{9}\eta^2 \tag{9}$$

$$S_F = (1-\eta)^2\left[2-(1-\eta)^2\right] \tag{10}$$

$$\eta = \frac{d_m}{d_p} \tag{11}$$

The parameters d_m and d_p are the diameter of a molecule and the diameter of a membrane's pore, respectively.

The model of Zeman and Wales [8, 9], similar to the SHP model, assumes that the pores have a uniform cylindrical diameter. Furthermore, parabolic velocity dependence in the pore is considered. With the assumption that transport of molecules through membrane is the transport of sphere through capillary, the reflection coefficient is represented by simply expression:

$$\sigma = 1 - \left(\eta(\eta-2)^2\right) \tag{12}$$

Because during the filtration the steric hindrance gives rise to a hydrodynamic lag in the membrane pores, Zeman and Wales, based on the experimental results, proposed modification of eq. (12) to:

$$\sigma = 1 - \left(\eta(\eta-2)^2\right)e^{-\alpha\eta^2} \tag{13}$$

where α is a dimensionless constant.

Log-normal model is the first from proposed models which assumes that pore size is not constant and the log-normal distribution for the pore sized is proposed in Ref. [10, 11]. In this model authors assumed that the only criterion of the transport of molecules through membranes' pores is their sizes. Thus only molecule with smaller diameter than the diameter of pore can permeate through pores in membrane filtration process. Some effects are negligible in this model: steric hindrance in the pores, hydrodynamic lag and contribution of diffusion to transport. With these assumptions and simplifications, the reflection coefficient is represented by expression:

$$\sigma(r^*) = \int_0^{r^*} \frac{1}{S_p\sqrt{2\pi}}\frac{1}{r}\exp\left(-\frac{\left[\ln(r)-\ln(\bar{r})\right]^2}{2S_p^2}\right)dr \tag{14}$$

In eq. (14) S_p is the standard deviation of the distribution of the pore size, $\bar{r}$ is a mean pore size.

Adapted version of the log-normal model is the model in which to the log-normal model the hydrodynamic lag is taken into account. Thus, it could be assumed that if the molecule has larger diameter than pore size than the 100 % retention is obtained. The partition retention is obtained in the case when the pore diameter is larger than the molecular diameter and could be explained by difference in velocity of molecule (v_m) and water in the pore (v_p). According to the Zeman and Wales model the ratio of these velocities can be calculated from the equation:

$$\frac{v_m}{v_p} = \exp\left(-\alpha\eta^2\right) \tag{15}$$

The combination of both models: log-normal and Zeman and Wales, allows calculating the reflection coefficient as:

$$\begin{aligned}\sigma(r^*) &= \int_0^{r^*} \frac{1}{S_p\sqrt{2\pi}}\frac{1}{r}\exp\left(-\frac{\left[\ln(r)-\ln(\bar{r})\right]^2}{2S_p^2}\right)dr \\ &+ \int_{r^*}^{\infty}\left(1-\exp\left(-\alpha\left(\frac{r^*}{r}\right)^2\right)\right)\frac{1}{S_p\sqrt{2\pi}}\frac{1}{r}\exp\left(-\frac{\left(\ln(r)-\ln(\bar{r})\right)^2}{2S_p^2}\right)dr \\ &= 1 - \int_{r^*}^{\infty}\exp\left(-\alpha\left(\frac{r^*}{r}\right)^2\right)\frac{1}{S_p\sqrt{2\pi}}\frac{1}{r}\exp\left(-\frac{\left(\ln(r)-\ln(\bar{r})\right)^2}{2S_p^2}\right)dr\end{aligned} \tag{16}$$

Independently of the using model to their experimentally validations the size of the molecules is necessary. For the calculation of the molecular diameter the HyperChem or Gaussian programs can be used successfully.

Van der Bruggen et al. [3] compared the experimental results with models described above by fitting the relevant equations to the experimental data using a least-squares method. They used three nanofiltration membranes NF70 (crosslinked aromatic polyamide), NTR 7450 (sulfonated polyethersulfone), UTC-20 (polyamide) to recovery the small organic molecules. Obtained results show that all models have deviation from experimental data. The main reason of that are too many simplifications. The both log-normal models gave better results than SHP model and the model of Zeman and Wales. Better fitting is observed for high value of TMP. Acceptable results of log-normal model, with deviation from experimental results up to 20 %, were presented by the same authors for separation of low molecular organic compounds from aqueous solution using nanofiltration NF70, NTR 7450 and UTC-20 membranes [12] They suggested that the log-normal model appeared to be most useful to predict reflection coefficients in practical applications. Moreover utility of these models to predict the retention specific active pharmaceutical ingredients (API's) from toluene, methylene chloride, and methanol using solvent resistant nanofiltration process are presented in the literature [13]. SHP model, the Zeman-Wales model, the Verniory model [14] and the log-normal model were used to calculate the pore diameters of membranes. The order of magnitude of estimated pore diameter is the same for each model, about 1 nm and it is compatible with experimental results.

Wherein, in Verniory model in cylindrical membrane pores the frictional drag force is included and the reflection coefficient can be calculated as:

$$\sigma = 1 - g\left(\eta\right) S_F \tag{17}$$

where

$$g\left(\eta\right) = \frac{1 - \frac{2}{3}\eta^2 \ - 0.2\eta^5}{1 - 0.76\eta^5} \tag{18}$$

$$S_F = \left(1 - \eta\right)^2 \left(1 - \left(1 - \eta\right)^2\right) \tag{19}$$

Martin-Orue et al. [15] used Zeman and Wales model in their study of nanofiltration process. It would not be surprising, but this was a study of the nanofiltration process of various charged amino acids and peptides. As was mentioned above, the Zeman and Wales model is the model for uncharged molecules. The theoretical retentions, estimated form the model, were different from the experimental results. Based on this results authors suggested that charge effect, both repulsion of coions and attraction of the counterions, was more important in description transport through membrane than size effects.

As was mentioned above (see eq. (6)) retention in membrane filtration is directly related to volumetric flux. Therefore, the membrane transport models could be used to describe the efficiency of separation in membrane process. The most popular is solution diffusion model (SD), solution-diffusion-imperfection model (SDI), preferential-sorption-capillary flow model (PSCF), Donnan exclusion model (DE) and extended Nernst–Planck model (ENP). In SD model [16] the main assumption is that solute and solvent dissolve and then diffuse through the homogeneous non-porous membrane due to chemical potential gradient. Therefore, the separation process occurs due to the difference in the solubility and diffusivities of compounds in the feed solution. The gradient (driving force of the process) results from concentration (due to concentration polarization) and pressure difference across the membrane. The SDI model is extension SD model. Model takes into account the pore flow. In the PSCF model, there is assumption that separation mechanism is based on surface phenomena and fluid transport through pores in the membrane. The membrane has such chemical properties that the sorption of solvent and repulsion of solutes are preferred. The Donnan exclusion model is proposed when a charged membrane is used in separation process of charged compounds. In this case concentration of opposite to membrane charge ions from the feed solution is higher and concentration of ions with the same charge as membrane is lower in comparison to the concentration in the bulk solution. Thus the counterions diffuse from the membrane phase to the bulk solution, while coion in the opposite direction.

The transports of ionic species through membrane, as well as their retentions are well described by the ENP equation [17–19]. This phenomenological model is also used for description of molecules transport through the charged membranes [20]. The model assumes each of the mechanisms described above. Both solubility and diffusivity of solute and solvent in the nonporous and homogeneous surface layers of the membrane due to the chemical potential gradient which is the result of concentration and pressure difference across the membrane, as well as transport of ions through pores with convective, diffusive and electrostatic migration forces are taken

into account. Electro neutrality between ions among each other and between ions in the solution and in the membrane are guaranteed by adding the Donnan condition. ENP equation is given by:

$$J_i = -D_{i,p}\frac{dc_i}{dx} - z_i c_i D_{i,p}\frac{F}{RT}\frac{d}{dx} + K_{i,c}c_i J_v \tag{20}$$

where J_i is the solute flux, $D_{i,p}$ – the hindered diffusivity, c_i – the solute concentration, z_i – the ion valence, F – the Faraday constant, Ψ – the electric potential, $K_{i,c}$ – the hindrance factor for convection.

The first term in eq. (20) represents the flux component due to the diffusion, the second term accounts for flux due to the Donnan potential, and the last term describes flux due to convection. The solution of this equation was discussed by Bowen and Mukhtar [21]. The hindered diffusion coefficient and the convective hindrance factor could be estimated from numerical calculations using the ratio of ionic radius over pore radius, and the bulk diffusion coefficient.

The solution of eq. (20), with following boundary conditions using $c_i = c_{m_i}$ for $x = 0$ and $c_i = c_{p_i}$ for $x = \Delta x$, allows calculating the retention according to the relationship [18]:

$$R = 1 - \frac{1-\sigma}{1-\sigma\cdot\exp\left[-\frac{(1-\sigma)J_v}{P_s}\right]} \tag{21}$$

where P_s is solute membrane permeability, σ – salt reflection coefficient, subscripts m and p in c – the concentration in membrane and permeate, respectively.

The ENP model was used to fit the experimental data of NaCl and $CuSO_4$ transport in nanofiltration process with polyamide membrane [17]. From the ENP model, with good agreement to the experimental results in different conditions ($R^2 \approx 0.99$), authors estimated diffusive and convective flow. Similar results for $Ca(NO_3)_2$, $Cd(NO_3)_2$, $Cu(NO_3)_2$ and $ZnCl_2$ rejection in process with nanofiltration Nanomax50 membrane (polyamide arylene on polysulfone support) were obtained by Chaabane et al. [18]. Authors showed good agreement between theoretical and experimental data.

In the literature, several authors proposed the combination of ENP equation with other equations whose describe the transport. By a combination of ENP model and film theory equations the thickness of the boundary layer, solute concentration of membrane surface and concentration profiles in the polarization layer could be estimated as proposed in Ref. [22]. By this approach three principal parameters are determined: reflection coefficient (σ), the solute membrane permeability (P_s) and the layer polarization thickness (δ). The authors' assumptions were verified on the experimental results of removal of phosphorus ions using nanofiltration membrane NF90 (polyamide thin-film composite with a microporous polysulfone supporting layer). The results showed that the convective transport dominated at higher values of TMP and pH, while diffusive transport dominated at higher temperature. The results from the model are in agreement with the experimental observations. Another approach was proposed by Hua et al. [23] Authors used ENP model and film theory to calculate the retention of xylo-oligosaccharides syrup in nanofiltration process using aromatic polyamide membrane ((HDS-12-2540). The model proposed very well fitted the experimental results. Two model parameters: reflection coefficient (σ) and the solute membrane permeability (P_s) were estimated by curving fitting using genetic algorithm method. Moreover, using steric-hindrance pore model (SHP) two parameters which describe the membrane structural were estimated – ratio of solute radius to pore radius (see eq. (8)) and ratio of effective membrane porosity to membrane thickness.

To clarify experimental results of membrane separation, authors support their work by quantum calculations, based on density functional theory (DFT). Zhao et al. [24] studied the role of calcium ions in the process of removal perfluorooctane sulfonate (PFOS) by nanofiltration using NF270 membrane (semiaromatic piperazine-based polyamide thin-film composite with a microporous polysulfone supporting layer.). The results indicated that with increasing calcium chloride concentrations in the feed solution the rejection of PFOS also increased. To explain these results authors checked the possible interaction between PFOS and calcium ions. Calculations were carried out using gradient-corrected DFT with the Becke three-parameter nonlocal exchange functional and the Lee–Yang–Parr correlation functional (i. e. B3LYP). The geometries of PFOS interacting with calcium ion were optimized using the 6-31G(d) basis set. Low-spin and restricted closed-shell formulae were applied during the structural optimization. The formation of $CF_3(CF_2)_7SO_3Ca^+$ structure was confirmed by DFT calculation. This structure with higher molecular polarity is favorable to interact with the charged membrane surface. Moreover calcium ions by neutralization PFOS anions (with formation $CF_3(CF_2)_7SO_3CaO_3S(CF_2)_7CF_3$) and the negative charged NF270 membrane promoted sorption of PFOS on membrane surface. Surface sorption and formation described above structure (Ca^{2+} ion linked with two PFOS molecules) caused the aggregation of PFOS at the surfaces and increase the size of the molecules (from 10.88 to 26.17 Å). Thus increase of retention could be explained by size exclusion. Moreover, Ca^{2+} could bridge the negatively charged membrane surface

and PFOS. It could cause enhancing the adsorption/deposition of PFOS on the membrane, which hinders the passage of water and PFOS molecules. The results obtained from DFT calculation were confirmed by SEM and AFM images. These images exhibited that with the increasing of calcium concentration, the membrane surface had more precipitation and higher surface roughness, and PFOS accumulation on the membrane increased, all off which correspond to flux decline and retention change.

DFT methods were used also to investigate the adsorption configurations of natural organic matter (NOM) compound on the nanofiltration, polyamide membrane surface [2]. The four compounds: p-coumaric acid (hydrophobic phenolic molecule), L-leucine (hydrophilic amino acid), acetic acid (nonionic hydrophilic carboxylic molecule), L-tryptophan (hydrophobic amino acid) and two types of membranes: NE90 (fully aromatic polyamide based on trimesoyl chloride and 1,3-benzenediamine) and NE70 (semi aromatic polyamide based on trimesoyl chloride and piperazine with polyvinyl chloride (PVA) coating) were considered. To calculation highest occupied molecular orbital (HOMO) and lowest unoccupied molecular orbital (LUMO) with frontier orbital gap were carried out with the B3LYP/6-31G* level theory. This method is helpful in estimated adsorption energy between organic molecules and the membrane materials, which is relative to retention of compounds in the process, as well as membrane fouling. The prediction of the interfacial phenomenon between compounds from feed solution and membranes could be relative to membrane fouling and retention. The compounds with high-energy gap have got higher tendency to adsorb on the membrane surface. Moreover, this tendency is depended on the kind of membrane's material (energy of bound). Kaewsuk and Seo [25] compared the results obtained by DFT calculation with experimental results and shoved good agreement between them. The experimental results showed that in the process of nanofiltration with the membrane NE90 the lower permeate flux and higher retention (especially carboxylic compound) were obtained in comparison to process with NE70 membrane. It could be explained by adsorption of organic compounds on the membrane surface. The calculation results confirmed these assumptions and showed that carboxylic compound has high-energy gap and tend to adsorb on the membrane surface than the other compounds (phenolic and acetic acid) and it bound higher energy with NE90 than NE70. Consistency of experimental and computational results indicates on possibility to predict the efficiency of membrane separation process by quantum calculations. Thus, without the experiments it can be assumed that the membrane will be or not suitable for retention of compounds considered. This is important at the planning stage of the synthesis and modification of the membrane surface as well as its selection for the process.

The novelty approach of rejection modeling of charged and uncharged organic compounds by nanofiltration and reverse osmosis membranes was presented by Khaouane et al. [26]. In their work authors used bootstrap aggregated neural networks (BANN) or bootstrap aggregated multiple linear regressions (BAMLR) to predict the value of retention. These methods are better than classical artificial neural networks (ANN) when only a limited amount of data is available. In this case, ANN model gives the result with significant errors. The aggregated neural network is a technique that improves the generalization ability of a model through training a number of neural networks and them combining them. Both BANN and BAMLR model are presented schematically in Figure 1. BANN model consists of several individual neural network models (INN) and BAMLR model – several MLR models, which are both developed to model the same relationship. Authors used results from literature and created database containing 436 rejections of 42 charged and uncharged organic compounds. From all results 350 data points (80 %) were used for the training phase, 43 points (10 %) for the validation step and 43 data points (10 %) for the testing phase of the model. The inputs model variables were divided into three groups which describe the compounds properties, membrane properties and process condition. To the first group belongs: molecular weight, compound hydrophobicity (logD), dipole moment, molecular length and equivalent molecular width. The membrane properties are described by the following inputs variable: sodium chloride salt rejection "SR (NaCl)" or magnesium sulfate salt rejection "SR($MgSO_4$)", the molar weight cut off, surface membrane charge (represents as zeta potential) and membrane hydrophobicity (represents as contact angle). The last group is: pH, TMP and temperature. The output variable in the model was rejection. The authors pointed out that the most commonly used parameter, the molar weight cut off, was insufficient alone to determine retention of charged and uncharged organic compounds by nanofiltration or reverse osmosis. In the case of RO process, with dense membrane, the most appropriate parameter is salt retention [27] while in NF process the molecular weight cut off and ionic retention of salts (mainly $MgSO_4$ "SR($MgSO_4$)" or NaCl "SR(NaCl)).

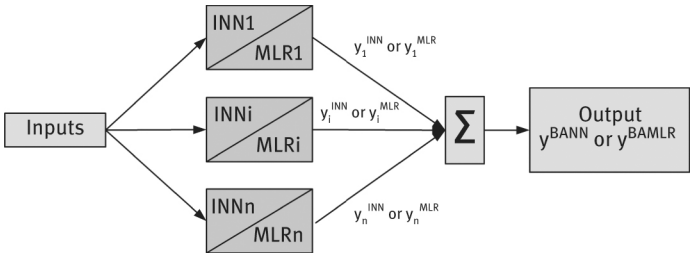

Figure 1: Schema of the bootstrap aggregated neutral networks (BANN) or bootstrap aggregated multiple linear regressions (BAMLR).

From the simulation, it can be concluded that BANN model is the best one to predict the rejection of charged and uncharged organic compounds in membrane filtration process, in comparison to the single neural network (SNN) and the BAMLR. The following results of the root mean squared errors were obtained 5.33 %, 6.45 % and 18.78 %, respectively.

Without using neural networks, the simple MLR was also proposed to modeling of RO/NF membrane rejections of pharmaceutical compounds and organic compounds [28]. In the statistical analysis 64 cases representing rejections of 14 compounds were considered. At first principal component analysis (PCA) was used to data reduction – replacement larger number of original variables (physical-chemical properties) by small number of derived variables to simplify subsequent analysis of the data. Then MLR was used to determine the strength of the relationship between a set of explanatory variables known as independent variables, and a single response or dependent variable using stepwise method for linear regression. Based on the principal component analysis results authors suggested that the most important parameters for prediction of membrane rejection were dipole moment, molar volume, hydrophobicity/hydrophilicity, molecular length and equivalent width. Molecular weight was found to be a poor variable to rejection simulation. MLR could predict well the rejection of uncharged molecules (R^2>95 %) while this method is not suitable to modeling the retention of charged molecules (R^2<60 %), due to the important influence of charge repulsion between the membrane and those charged compounds.

1.2 Membrane fouling

Generally, during the membrane process the decrease of the permeate flux is observed. This is mainly caused by the substances deposition on the membrane surface or into membrane pores. Depends of the kinds of containments two processes can occur – fouling or scaling. Fouling of membranes is due to the suspended or emulsified materials, such as colloidal (clay, flocs, surfactants), biological (bacteria, fungi), organic (oils, polyelectrolytes, humics) compounds. The mineral precipitates, mainly calcium, cause the scaling effect. When the concentration of salts in the process is above solubility equilibrium the deposition of particles on a membrane in the form of solid is occurred [29].

Typical relationship between permeate flux and time of flirtation process, with three stage, is presented in Figure 2 [30]. Stage (I) is the rapid reduction of flux in relation to flux obtained for pure water filtration. The next stage is slowly decreasing the flux in the filtration process. This stage exists always in membrane fouling system regardless the operation conditions. In stage (III) flux is in a steady state.

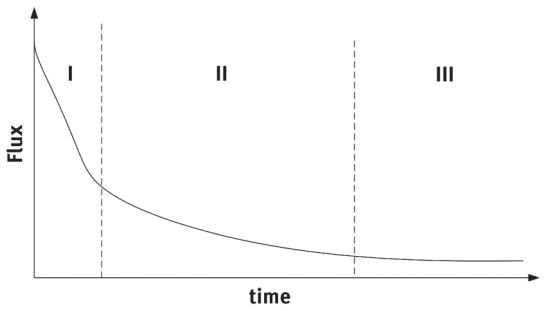

Figure 2: Schema of flux reduction: (I) initial rapid, (II) long-term gradual flux decline and (III) steady-state flux.

Membrane fouling is negative phenomenon in membrane technology. It increases the costs of the process by increasing energy consumption, system down time, necessary membrane area and construction, labor, time and material costs for backwashing and cleaning processes.

1.2.1 Fouling – experimental methods

Fouling results in higher membrane resistance and affects permeate quality. The simplest experimental method of fouling description is to measure of permeate flux decreasing during the process. The flux reduction can be related to fouling using mass transfer and fluid mechanics concepts. Of course, such approach allows only to determine whether the phenomenon of fouling occurs or not, without any explanation of it. To characterize fouling on membrane is very important to identify where it is occurring and how much is being deposit. Several experimental methods are proposed. Lots of them are similar to these used in characterization of membrane structure (described in detail in Section 2.2). For example scanning electron microscopy (SEM), environmental scanning electron microscopy (ESEM) transmission electron microscopy (TEM), confocal microscory, radiolabelling, X-ray photoelectron spectroscopy (XPS) and infrared spectroscopy (IR) are very helpful to see the place of foulants deposit [31–34] However internal deposition with the pores and low foulant levels remain difficult to detect. The fouled membranes can be also analyzed for any changes in pore size distribution using a polydisperse dextran solution sieving test [35].

1.2.2 Fouling modeling

To explain the flux decline many different models have been proposed in the literature. The most often used ones are: A. the standard blocking model, B. intermediate blocking model, C. complete blocking model and D. cake filtration model (Figure 3) [36, 37]. These models are successfully evaluated to explain fundamental mechanisms involved in flux decline during filtration process as microfiltration, ultrafiltration [30], nanofiltration and reverse osmosis [38].

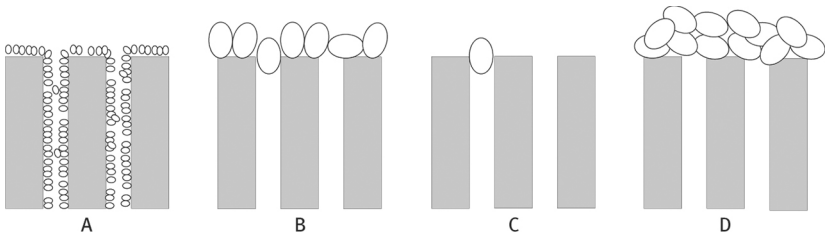

Figure 3: Schema of fouling models: A. Standard blocking model, B. Intermediate blocking model, C. Complete blocking model and D. Cake filtration model.

Standard blocking model assumes that particles accumulate inside the membrane on the pore walls and the resulting smaller size of pores the membrane's permeability is reduced. In the model of intermediate blocking the reason of the decreasing of flux is interpreted by the accumulation portion of particles in the pores, while the rest accumulate on the top of the deposited particles. In the complete blocking model there is assumption that particles are larger than the pore size and can seal of the membrane. Cake filtration model is based on the hypothesis that the particle accumulation on the membrane surface, in a permeable cake, causes the thickness increasing.

These mechanisms are helpful in interpretation of experimental results. In the standard blocking model the time dependency of volume flow (J_V) is expressed as [37]:

$$J_V(t) = \frac{J_V(0)}{(1 + B \cdot t)^2} \tag{22}$$

where B is equal to:

$$B = K_B \cdot u_0 \tag{23}$$

K_B is the reduction in the cross section area of the pores per unit of total permeates volume, caused by the adsorption on the pores walls. Parameter u_0 is the mean initial velocity of the filtrate and is calculated according to the relationship:

$$u_0 = \frac{J_V(0)}{A_0} \tag{24}$$

where A_0 is a porous surface of the membrane.

Total permeate volume is changed with time and is expressed as:

$$V(t) = \frac{J_V(0) \cdot t}{1 + B \cdot t} \tag{25}$$

Bowen et al. [37] suggested that characteristic equation of the blocking processes is given by:

$$\frac{d^2t}{dV^2} = \frac{2B}{\sqrt{J_V(0)}} \left(\frac{dt}{dV} \right)^{3/2} \tag{26}$$

The same considerations were made for other fouling models and general pattern of the characteristic equation was proposed:

$$\frac{d^2t}{dV^2} = \alpha \left(\frac{dt}{dV} \right)^{\beta} \tag{27}$$

Values of parameters α and β are depended of the fouling model according to the Table 1, as was proposed in [37].

Table 1: Parameters in equation (27).

Fouling model	α	β
Standard	$\left(2K_B/A_0^{1/2}\right) \cdot u_0^{1/2}$	1.5
Intermediate	K_A/A_0	1
Complete	$K_A \cdot u_0$	2
Cake	$(R_r K_C/A_0^2) \cdot u_0^{-1}$	0

In Table 1, K_A is the membrane surface blocked per unit of total volume permeated through the membrane; K_C is area of the cake per unit of permeate volume; R_r is the hydraulic resistance of the cake divided by the resistance of the initial or clean membrane ($R_r = R_c/R_0$).

From the experimental results the plots d^2t/dV^2 versus dt/dV can be obtained and from them the values of parameter β can be calculated. It is possible to determine the assumed fouling model from the values of the β parameters read from the Table 1. Therefore, theoretically, it is a very simple method of defining fouling on membranes. However, it should take into account that these models have a number of simplifications, which may affect their accuracy. Thus, there are several other simplistic, macroscopic mathematical models to predict flux decline, very often as a combination of above models presented [39–41]. The main problem of these approaches is that there is no certainty that estimated parameters for one set of membrane operating conditions can be applied to another set. Moreover, commonly used membrane blocking models (i. e .standard, intermediate, complete or cake blocking) do not adequately describe fouling phenomena for membranes. Instead, of one model the phenomena can occur in successive or simultaneous coexistence [42]. This causes that experimental validation is necessary for new process conditions (i. e. kind of membrane, composition of the feed solution or operating conditions). For example there are few propositions of description of fouling for the filtration process of the same compounds – bovine serum albumin (BSA). Ho and Zydney [43] developed a mathematical model (combined pore blockage and cake filtration model) for the microfiltration of protein. The model showed excellent agreement with the experimental data obtained during the filtration of BSA solutions operated at constant pressure through polycarbonate membrane. Simply model based on deposition mechanism and validation of microfiltration process of BSA using polyethersulfone membrane at different pH and pressures and using cellulose acetate was described in [44] and [45], respectively. Bolton et al. [46, 47] proposed combined caking and complete blockage models of membrane fouling in the microfiltration process of BSA with PVDF membrane. Duclos-Orsello et al. [48] showed that fouling model depends of the kind of membrane material for the same feed solution containing BSA. The model predictions were validated by experimental results from polystyrene microsphere solution through PCTE membranes (representing complete external fouling), prefiltered BSA solution through Durapore membranes (representing internal fouling), and standard BSA solution through Durapore membranes.

Because macroscopic models have their limitations, Wessling [49] proposed two-dimensional stochastic modeling of membrane fouling. The algorithm assumes the deposition of a particle with defined length on

a microfiltration membrane having a cylindrical pore. Particle motion is described by diffusion limited aggregation (DLA) model. In DLA, there is a stationary sees particle on a lattice and second mobile particle at a random location on the gird. This second particle walks on the lattice until it meets the seed particle and becomes immobile. A new mobile particle is added at a new random position. This new particle has got new walks until meeting the immobile cluster. Schematic drawing representing the basic simulation algorithm is presented in Figure 4.

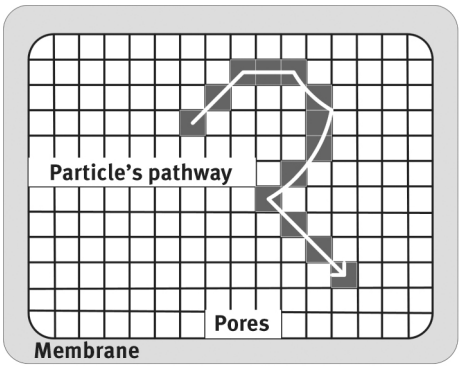

Figure 4: Schema of simulation algorithm.

The effect of pore diameter, flow conditions, membrane thickness on the permeate flux, resistance of membrane was simulated by this method. Moreover model is helpful to description of retention characteristics. Counting the numbers of particles passing the pore as a function of the number of particles deposited allows characterizing the change in retention behavior. As a result of simulation, presented in work [49], it could be concluded that the aggregate density above the flat adsorption surface was bigger in comparison to the aggregate density above the pore opening. Two distinct regimes are visible during the flux decline as a function of number of particles deposited. Initially, in the filtration process, the flux decline is determined by internal fouling and membranes with the same initial flux but different pore diameter show different flux decline: the membrane with the smaller pore has a more rapid flux decline.

As an alternative to the above-described simple mathematical and stochastical models, often based on the experimental observation, a completely different approach based on quantum methods is proposed. This method allows describing the interaction between compounds of foulants and membrane's material. For example in the process of ultrafiltration of proteins the non-covalent intermolecular interactions are responsible for adsorption and the packing of macromolecules, like proteins, on the membrane surface [50]. The distribution of the electrostatic charges on the protein surface controls the interactions between protein molecules, thus it affects the adsorption on the membrane. This is where the Quantum Mechanics (QM) approach, based on DFT, is useful – methods for determination of the partial charges on the atoms of any molecular system. De Luca et al. [50] proposed to use quantum mechanics approaches to calculate the effective diameter of bovine serum albumin (BSA) and the electrostatic surface charges (by Lowdin's approach and the ElectroStatic Potential method (ESP)). Lodwin's approach is based on the weighing of each atomic orbital belonging to the overall molecular orbitals. ESP method is based on the fitting of molecular quantum mechanics electrostatic potentials obtained from the electron density function and the nuclear geometry. Authors of citied work used in their calculations the Hybrid energy functional, X3LYP in conjunction with a Gaussian-triple Double-ζ orbital basis set added with polarization function (6-311 g*). Results obtained from the quantum calculation were used as the starting point for multi-scale model based on unsteady-state mass balance equation. Solution of the mass balance as well as force balances for each the layers constituting the deposit allows to estimate the mass of the particles constituting the deposit in the membrane and deposit specific resistance. Presented model was experimentally validating (ultrafiltration of BSA under different TMP using polyethersulfone membrane). A rather good agreement was obtained only after about 20 min of process (end time – 1 h). At the beginning of the process percentage errors exceeded of model 20 %.

By using models described above, permeate flux can be predicted for various process variables, such as such as TMP, composition of the feed solution, kind of membrane (material and pore size). However, there are various complex phenomena effecting flux in a membrane filtration process and until now, none of the developed models were fully and satisfactorily described the membrane filtration process. Thus, to predict membrane fouling and permeate flux decay as a function of process operating parameters the empirical models, based on ANN, are proposed briefly in literature [51–56]. ANN, the so-called "black-box" model, is simple and effective predictive instrument for solving non-linear problems. Generally in citied literature the permeate flux is ANN output, while the operating variables are ANN input (Figure 5). During the training process of the networks the four steps are followed: i. analysis and elaboration of the experimental data; ii. building of the neural model;

iii. training of the network and post-training analysis; iv. post-simulation analysis. The results obtained from ANN modeling showed the excellent agreement between experimental data and predicted values of permeate flux vs. time.

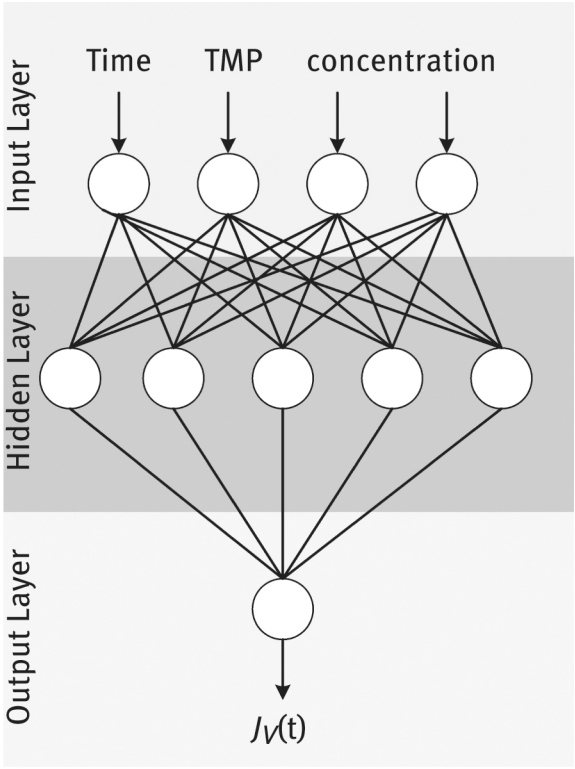

Figure 5: Architecture of neural networks.

Liu and Kim [54] compared the performance of purely mathematic and mechanical model (see Figure 3) with the so-called "black-box" ANNs model. The models were evaluated based on bench-scale experiments with synthetic water (mixture of Georgia kaolinite, alumina, Aldrich humic acid (AHA), $NaHCO_3$, $CaCl_2$) in this study using PVDF hollow fiber membrane. Authors used all blocking models – standard, intermediate, complete blocking model and cake filtration model. Unfortunately, models could not fit the experimental data well in whole experimental period, but they fitted much better in separate specific experimental periods. The combined cake-complete and the cake-intermediate models demonstrated relative high consistency with experimental TMP data. The excellent agreement between experimental data and prediction has been obtained with ANN model what confirmed the results presented in literature [51–53].

Interesting solution of fouling modeling was proposed by Chew et al. [57] A novel approach combining first principle equation of Darcy's law on cake filtration and ANN predictive models were utilized to represent the dead-end ultrafiltration process. The first principle model allows establishing the relationship between permeate flux, resistance and TMP. ANN model was used as an alternative to predict the specific cake resistance which requires complicated laboratory analysis procedures using the conventional method. This hybrid model allows to rapid estimation of the specific cake resistance with common on-line data such as feed water turbidity, filtration time and TMP.

Presented above consideration suggests the potential application of model to characterization of efficiency of membrane separation processes.

2 Membrane characterization

2.1 Introduction

Type of the membrane and its properties plays very important role in membrane technology. Membrane material, with specific morphologies and transport properties, determines in which process it can be used. Membrane selection depends on a variety of factors, including the composition of the feed solution, operating parameters (temperature, pH, pressure etc.), application type, and separation goals.

Membranes are made from inorganic (ceramic, glass, metal) or organic materials (polymer). Usually, the synthetic, polymeric membranes are used in the membrane separation processes. Their classification by the membrane morphology, geometry, preparation method is presented in Figure 6 [58].

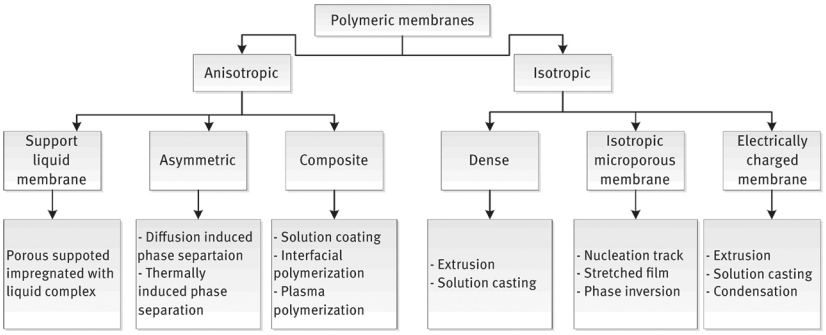

Figure 6: Polymeric membrane classification.

In terms of morphology polymeric membranes are classified into anisotropic and isotropic membranes. Anisotropic membranes are layer structures. It is means that the porosity and pore size are changing in cross-section (Figure 7) and thin surface layer is supported on a thick microporous substrate. The skin layer is responsible for separation while porous support provides the mechanical strength. Nonporous dense membranes, isotropic microporous membranes, and electrically charged membranes are the examples of isotropic membranes. Dense membranes are made by one kind of polymer without porous, isotropic microporous membranes have randomly distributed interconnected pores. Electrically charged membranes (anion-exchange or cation-exchange membranes) have got dense or microporous structures, with fixed positive or negatively charged ions.

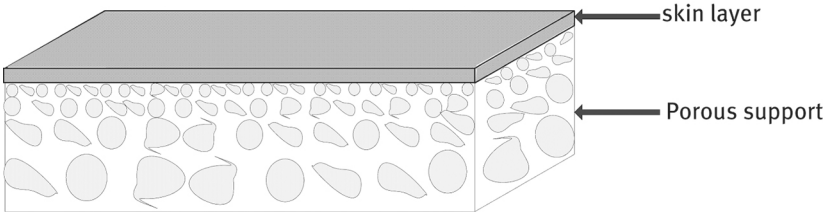

Figure 7: Layer structure of membrane.

Depending of the kind of membranes (their morphology, structure) different method of their fabrication (see Figure 6), experimental characterization and modeling approach is proposed, which is described in detail in the following sections.

Most commercial membranes are formed via casting process called immersion precipitation [59]. This type of membranes is used in such processes as reverse osmosis, ultrafiltration, gas separations and pervaporation. In this technique, a polymer solution (polymer with solvent) is immersed into a precipitation bath, which is a non solvent to the polymer, or a mixture non-solvent/solvent. After immersion, the solvent from the polymer solution diffuses into the precipitation bath, whereas the non-solvent diffuses into the polymer solution. The combination of phase separation and mass transfer affects the membrane structure [60–62]. Figure 8 represents schematically the immersion precipitation process [63, 64]. In this technique lots of parameters affect on the final products such as choice of the polymer, solvent, non-solvent and precipitation bath composition as well as casting conditions such as temperature, evaporation time and concentration of the casting solution [65]. Consequently, the great sort of morphologies of membranes can be obtained – from non-porous structures to porous structures of the sponge type and of the finger/macrovoid type. Because membranes with various morphologies show different mechanical and transport properties, the ability to predict final membrane structures through analytical or computational methods is very important and helpful in process optimization. The deep understanding to phase inversion process is valuable to effectively adjust and control the membrane structure and functionalities for antifouling, selectivity and flux.

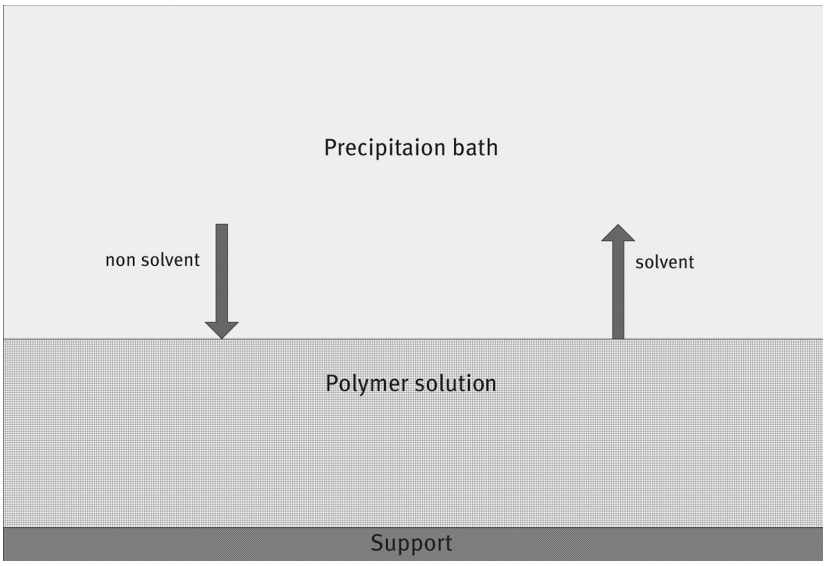

Figure 8: Schema of the immersion precipitation process.

In modeling of such type of membrane formation few methods are reported. These approaches are presented in Section 2.3.

2.2 Experimental characterization of membranes

The characterization of membranes is important for membrane selection, membrane process diagnosis, and new membrane material design. Their description can be classified into three categories: physical morphology, chemical composition and membrane fouling characterization. The characterization of membrane depends on its morphology [66]. Because, mainly, the porous membranes are used, the typical way of characterizing the membrane is to determine pore size and pore size distribution of the membrane. In the case of dense membranes the parameters of their characterization are volume size and free volume distribution [67]. Moreover it is very important to characterize of membrane surface morphology for both porous and dense membrane. The knowledge about the chemical composition of the membrane surface is necessary to know the chemical changes of the surface before and after surface modification or to know what kind of foulants is adhered to the membrane surface. Some experimental methods of membrane characterization proposed in literature are listed below.

Pore size distribution measurements (porous membranes) [67–75]:

- bubble gas transport method (bubble point method) – measurement of the pressure necessary to blow gas (mainly air) through porous membrane filled with water;
- mercury porosimetry – variation of above method, instead of water the mercury is used to fill membrane;
- adsorption-desorption method – measurements of adsorbed gas (mainly nitrogen) versus relative pressure (pressure/saturation vapor pressure of the adsorbent);
- permporometry (gas liquid equilibrium method) – measurements of the gas flux through the membrane, method based on the controlled blocking of pores by condensation of vapor;
- thermoporometry – performance of the freezing or melting thermograms using differential scanning calorimeter (DSC);
- water permeability – measurements of hydraulic permeability ($L_p = \frac{J_V}{TMP}$, where J_v is the permeate flux, TMP – transmembrane pressure) and calculate the pore radius using capillary pore diffusion model and Hagen-Poiseuille equation;
- electron microscopy (scanning electron measurements (SEM), transmission electron microscopy (TEM), scanning transmission electron microscopy (STEM), field effect scanning electron microscopy (FESEM), atomic force microscopy(AFM)) – methods for the viewing of cross sections of membranes, which is helpful for analyzing of pore size distributions;

– nuclear magnetic resonance (NMR) – methods based on comparison between the NMR characteristics of a material trapped within a porous network depending on whether it is in the liquid or solid state.

Characterization of free volume size and free volume distribution (dense membranes) [67, 76–79]:

– density measurements and the Bondi group contribution theory – methods based on difference between the sample's weight in air and in a nonsolvent with known density; from the density data the fractional free volume (FFV) can be calculated from equation: $FFV = \frac{V-1.3V_w}{V}$, where $V = \frac{1}{\rho}$ is the polymer's specific volume, ρ is the polymer's density and V_w is the estimated van der Waals volume calculated by the group contribution method of Bondi [76];

– scattering methods (small-angle X-ray scattering (SAXS), small-angle neutron scattering (SANS)) – methods for determination of volume or open cavities in membrane materials;

– positron annihilation spectroscopy (PAS) – measurements of positron lifetime and doppler broadening [77];

– wide-angle X-ray diffraction (WAXD) – the corresponding d-spacing values, which provide a measure of intersegmental distances between polymer backbones, is calculated from the diffraction peak maximum through the Bragg equation: $d = \frac{\alpha}{2sin\theta}$, where α is the wavelength of the radiation and 2θ is the angle of maximum intensity in the amorphous halo exhibited by the polymer [78];

– ellipsometry – measure the small changes in index of refraction [79];

– sorption and transport of low-molecular-weight molecules – method based on comparison of mass transfer of low-molecular-weight molecules with known properties through the membrane.

Membrane surface morphology measurements (dense and porous membranes) [58, 80]:

– microscopic method (scanning electron microscopy (SEM), transmission electron microscopy (TEM), atomic force microscopy (AFM) or X-ray photoelectron microscopy (XPS)) – technique allowing to get a tri-dimensional image of membrane surface;

– spectroscopic method (Infrared (IR) and Fourier transform infrared (FTIR) spectroscopy, Raman spectroscopy, electron spin resonance (ESR), nuclear magnetic resonance (NMR), wide angle X-ray scattering (WAXS), photoelectron spectroscopy (XPS), small angle neutron scattering (SANS), positronium annihilation lifetime spectroscopy (PALS), ultrasonic spectroscopy);

– differential scanning calorimetry (DSC);

– thermogravimetry (TGA);

– contact angle measurements – characterization of membrane hydrophilic/hydrophobic properties, its wettability;

– zeta potential measurements – technique to determine surface charge of membrane.

Polymer membrane, during the process, can swell. This phenomenon depends on the kind of polymer materials. Among experimental methods of characterization of membrane swelling there are very simple ones – like comparison of weight or thickness between dry and wet membrane [81]. Moreover the adaptations of techniques used in morphology characterization are proposed: thermoporometry [82], microscopy techniques [83] (SEM, TEM, fluorescence microscopy), spectroscopy methods (spectroscopic ellipsometry [84], Raman and high-resolution magic angle spinning NMR spectroscopy [85]), X-ray powder diffraction.

2.3 Calculation method of membrane characterization

To predict the structural changes of the effective layer for membrane prepared under different conditions the two-parameter model of ENP equation (see Section 1.1, eq. (20)) is proposed [17]. This method is generally used for modeling the mass transport in terms of diffusive and connective flow, but indirectly could be helpful in characterization of membranes morphology, independent of the way of their preparation. In citied work authors prepared thin film composite polyamide membrane with microporous polysulfone support under different trimesoyl chloride (TMC) content and different reaction time. Depending of the TMC concentration as well as reaction time different membranes were obtained, i. e. high concentration of TMC – membrane with

higher thickness and diffusion resistance, long reaction time – membrane with narrower pore size. The proposed model very well described the experimental results. The same, ENP model was proposed by Diaper et al. [86] to develop new polyacrylic acid based membranes. The experimental results (rejection and permeate flux) of separation single electrolyte solutions by nanofiltration were interpreted based on ENP model. This approach let to predict the effective membrane charge density, porosity and thickness of membrane. Haasan et al. [87] proposed the combination of ENP equation with other equations to characterize the asymmetric, nanofiltration membrane. At first, based on pore flow, SD and ENP equations the modeling of experimental data (rejection) was done. Then the membranes parameters such as reflection coefficient, solute permeability and steric hindrance effects were estimated using Spielger–Kedem equations. Moreover, SHP model and Teorell–Meyer Sievers (TMS) model were proposed to estimate effective pore radius, effective charge density and ratio of effective membrane thickness to membrane porosity. From the modeling results, it was found that the polymer concentration can influence the membrane performances by varying of structural details. These conclusions were supported by the observation using scanning electron microscopy (SEM).

Because, as mentioned in Section 2.1, mainly membrane are prepared via phase inversion thus studies of thermodynamics and kinetics of this process, as well as computational method of membrane characterization are described briefly in literature. To calculation of thermodynamics phase diagrams of the system of polymer-solvent-nonsolvent (see Figure 8) few approaches are proposed: Flory–Huggins theory [88], binodal of ternary system with the consideration of the concentration dependence on the interaction parameters [89] and constant specific volume formulations [90]. Also, to calculation of kinetics of phase inversion some methods are presented in literature: simply mass transfer model known as Cohen's model [91] with assumption of equilibrium boundary condition at the interface between polymer solution and coagulation bath; extended Cohen's model by interface diffusion and frictional coefficients for the components [92] and by spinodal decomposition [93]; dissipative particle dynamics (DPD) simulation method [94].

Moreover, there is possibility to simulate precipitation process using multi-phase and multi-component Lattice–Boltzmann (LB) model to simulate precipitation process [95]. Generally, LB method is a mesoscopic model using to describe the macroscopic behavior of fluid flows. This method allows simulating a time-dependent structural formation during the membrane casting process of immersion precipitation. Two-dimensional (2D) simulation very well characterizes asymmetric membrane formation such as membrane compaction and formation of a selective skin layer. Moreover, the simulation of viscosity and forcing interactions effect on the final membrane structure agree with the experimental reports. Zhou and Powell [96] extended the simulation to 3D. They used ternary Cahn–Hilliard formulation incorporating a Flory–Huggins homogeneous free energy function to simulate the liquid–liquid demixing stage of the immersion precipitation process, which determines much of the final morphology of membranes. To simulation of actual membrane fabrication conditions in 2D and 3D authors used two-layer polymer–solvent/non-solvent as initial conditions. Moreover, this system is coupled with the Navier–Stokes equations to model hydrodynamics in 2D system. The model results were similar to experimental data. He et al. [97] proposed simulation with Monte Carlo method applying polymer bond fluctuation lattice model with the exchange algorithm using probability density. This method allows simulating the open and wide diffusion layer in coagulation bath.

To characterize the polymer materials DFTs also can be applied. DFT is able to account for microscopic details such as the molecular excluded-volume effects, associating interactions, van der Waals attraction, Coulomb forces, and inter- and intra- molecular correlations that are important for understanding interactions of polymers with other substances [98]. The numerical results show that the DFT predictions are in good agreement with experiments and molecular simulations for the polymer structure and surface properties. Although authors used DFT to explore the antifouling properties of polymer brushes and polymer nanocomposites, this method could also be used in polymer membrane characterization.

Presented above consideration suggests the potential application of model described to process design for optimizing membrane morphology and performance.

Funding

This research was supported with 03/32/DS-PB/0701 grant.

References

[1] Van den Berg GB, Smolders CA. Diffusional phenomena in membrane separation processes. J Membr Sci 1992;73:103–118.
[2] Kaewsuk J, Seo GT. Computational study of NF membrane removal in rejection of specific NOM compounds. Desalination Water Treat 2013;51:31–33, 6218–23.

[3] Van der Bruggen B, Schaep J, Wilms D, Vandecasteele C. A comparison of models to describe the maximal retention of organic molecules in nanofiltration. Sep Sci Technol 2000;35:169–182.
[4] Spiegler KS. Thermodynamics of hyperfiltration (reverse osmosis): criteria for efficient membranes. Desalination 1966;1:311–326.
[5] Nakao SI, Kimura S. Models of membrane transport phenomena and their applications for ultrafiltration data. J Chem Eng Jpn 1982;15:200–205.
[6] Mehiguene K, Garba Y, Taha S, Gondrexon N, Dorange G. Influence of operating conditions on the retention of copper and cadmium in aqueous solutions by nanofiltration: experimental results and modeling. Sep Purif Technol 1999;15:181–187.
[7] Anderson JL, Quinn JA. Restricted transport in small pores: a model for steric exclusion and hindered particle motion. Biophys J 1974;14:130–150.
[8] Zeman L, Wales M. Steric rejection of polymeric solutes by membranes with uniform pore size distribution. Sep Sci Technol 1981;16:275–290.
[9] Zeman L, Wales M. Polymer solute rejection by ultrafiltration membranes, Synthetic Membranes: volume II. Washington, DC: ACS, 1981, Chapter 23:411–434.
[10] Zydney AL, Aimar P, Meireles M, Pimbley JM, Belfort G. Use of the log-normal probability density function to analyze membrane pore size distributions: functional forms and discrepancies. J Membr Sci 1994;91:293–298.
[11] Bowen WR, Welfoot JS. Modelling of membrane nanofiltration – pore size distribution effects. Chem Eng Sci 2002;57:1393–1407.
[12] Van der Bruggen B, Vandecasteele C. Modelling of the retention of uncharged molecules with nanofiltration. Water Res 2002;36:1360–1368.
[13] Geens J, De Witte B, Van der Bruggen B. Removal of API's (Active Pharmaceutical Ingredients) from organic solvents by nanofiltration. Sep Sci Technol 2007;42:2435–2449.
[14] Verniory A, Dubois R, Decoodt P, Gassee JP, Lambert PP. Measurement of permeability of biological membranes – application to glomerular wall. J Gen Physiol 1973;62:489–507.
[15] Martin-Orue C, Bouhallab S, Garem A. Nanofiltration of amino acid and peptide solutions: mechanisms of separation. J Membr Sci 1998;142:225–233.
[16] Wijmans JG, Baker RW. The solution-diffusion model: a review. J Memb Sci 1995;107:1–21.
[17] Ahmad AL, Ooi BS. Characterization of composite nanofiltration membrane using two-parameters model of extended Nernst–Planck equation. Sep Purif Technol 2006;50:300–309.
[18] Chaabane T, Taha S, Ahmed T, Maachi R, Dorange G. Coupled model of film theory and the Nernst–Planck equation in nanofiltration. Desalination 2007;206:424–432.
[19] Kumaran M, Bajpai S. Application of extended Nernst Planck model in nanofiltration process – A critical review. Int J Eng Res Rev 2015;3:40–49.
[20] Tsuru T, Nakao SI, Kimura S. Calculation of Ion rejection by extender Nernst-Planck equation with charge reverse osmosis membranes for single and mixed electrolyte solutions. J Chem Eng Jpn 1991;24:511–517.
[21] Bowen WR, Mukhtar H. Characterization and prediction of separation performance of nanofiltration membranes. J Membr Sci 1996;112:263–274.
[22] Cathie Lee WP, Mah SK, Leo CP, Wu TY, Chai SP. Phosphorus removal by NF90 membrane: optimization using central composite design. J Taiwan Inst Chem Eng 2014;45:1260–1269.
[23] Hua X, Zhao H, Yang R, Zhang W, Zhao W. Coupled model of extended Nernst–Planck equation and film theory in nanofiltration for xylo-oligosaccharide syrup. J Food Eng 2010;100:302–309.
[24] Zhao C, Zhang J, He G, Wang T, Hou D, Luan Z. Perfluorooctane sulfonate removal by nanofiltration membrane the role of calcium ions. Chem Eng J 2013;233:224–232.
[25] Kaewsuk J, Seo GT. Verification of NOM removal in MIEX-NF system for advanced water treatment. Sep Purifi Technol 2011;80:11–19.
[26] Khaouane L, Ammi Y, Hanini S. Modeling the retention of organic compounds by nanofiltration and reverse osmosis membranes using bootstrap aggregated neural networks. Arab J Sci Eng 2017;42:1443–1453.
[27] Kimura K, Toshima S, Amy G, Watanabe Y. Rejection of neutral endocrine disrupting compounds (EDCs) and pharmaceutical active compounds (PhACs) by RO membranes. J Membr Sci 2004;245:71–78.
[28] Yangali-Quintanilla V, Sadmani A, McConville M, Kennedy M, Amy G. A QSAR model for predicting rejection of emerging contaminants (pharmaceuticals, endocrine disruptors) by nanofiltration membranes. Water Res 2010;44:373–384.
[29] Warsinger DM, Swaminathan J, Guillen-Burrieza E, Arafat HA, Lienhard VJ. Scaling and fouling in membrane distillation for desalination applications: a review. Desalination 2015;356:294–313.
[30] Song L. Flux decline in crossflow microfiltration and ultrafiltration: mechanisms and modeling of membrane fouling. J Membr Sci 1998;139:183–200.
[31] Chan R, Chen V. Characterization of protein fouling on membranes: opportunities and challenges. J Membr Sci 2004;242:169–188.
[32] Maruyama T, Katoh S, Nakajima M, Nabetani H, Abbott TP, Shono A, et al. FT-IR analysis of BSA fouled on ultrafiltration and microfiltration membranes. J Membr Sci 2001;192:201–207.
[33] Rabiller-Baudry M, Le Maux M, Chaufer B, Begoin L. Characterization of cleaned and fouled membrane by ATR–FTIR and EDX analysis coupled with SEM: application to UF of skimmed milk with a PES membrane. Desalination 2002;146:123–128.
[34] Reichert U, Linden T, Belfort G, Kula MR, Thommes J. Visualizing protein adsorption to ion-exchange membranes by confocal microscopy. J Membr Sci 2002;199:161–166.
[35] Bakhshayeshi M, Kanani DM, Mehta A, Van Reis R, Kuriyel R, Jackson N, et al. Dextran sieving test for characterization of virus filtration membranes. J Membr Sci 2011;379:239–248.
[36] Sampath M, Shukla A, Rathore AS. Modeling of filtration processes – microfiltration and depth filtration for harvest of a therapeutic protein expressed in pichia pastoris at constant pressure. Bioeng 2014;1:260–277.
[37] Bowen WR, Clavo JI, Hernández A. Steps of membrane blocking in flux decline during protein microfiltration. J Membr Sci 1995;101:153–165.

[38] Mohammadi T, Kazemimoghadam M, Saadabadi M. Modeling of membrane fouling and flux decline in reverse osmosis during separation of oil in water emulsions. Desalination 2003;157:369–375.
[39] Kim J, Di Giano FA. Fouling models for low-pressure membrane systems. Sep Purif Technol 2009;68:293–304.
[40] Miller DJ, Kasemset S, Paul DR, Freeman BD. Comparison of membrane fouling at constant flux and constant transmembrane pressure conditions. J Membr Sci 2014;454:505–515.
[41] Huang H, Young T, Jacangelo JG. Unified membrane fouling index for low pressure membrane filtration of natural waters: principles and methodology. Environ Sci Technol 2008;42:714–720.
[42] Jacob K, Pradanos P, Calvo JI, Hernández A, Jonsson G. Fouling kinetics and associated dynamics of structural modifications. Colloids Surf A 1998;138:173–183.
[43] Ho CC, Zydney AL. A combined pore blockage and cake filtration model for protein fouling during microfiltration. J Coll Interface Sci 2000;232:389–399.
[44] Velasco C, Ouammou M, Calvoa JI, Hernández A. Protein fouling in microfiltration: deposition mechanism as a function of pressure for different pH. J Coll Interface Sci 2003;266:148–152.
[45] Sun X, Kanani DM, Ghosh R. Characterization and theoretical analysis of protein fouling of cellulose acetate membrane during constant flux dead-end microfiltration. J Membr Sci 2008;320:372–380.
[46] Bolton GR, La Casse D, Kuriyel R. Combined models of membrane fouling: development and application to microfiltration and ultrafiltration of biological fluids. J Membr Sci 2006;277:75–84.
[47] Bolton GR, Boesch AW, Lazzara MJ. The effects of flow rate on membrane capacity: development and application of adsorptive membrane fouling models. J Membr Sci 2006;279:625–634.
[48] Duclos-Orsello C, Li W, Ho CC. A three mechanism model to describe fouling of microfiltration membranes. J Membr Sci 2006;280:856–866.
[49] Wessling M. Two-dimensional stochastic modeling of membrane fouling. Sep Purif Technol 2001;24:375–387.
[50] De Luca G, Bisignano F, Paone F, Curcio S. Multi-scale modeling of protein fouling in ultrafiltration process. J Membr Sci 2014;452:400–414.
[51] Curcio S, Scilingo G, Calabrò V, Iorio G. Ultrafiltration of BSA in pulsating conditions: an artificial neural networks approach. J Membr Sci 2005;246:235–247.
[52] Shetty GR, Chellam S. Predicting membrane fouling during municipal drinking water nanofiltration using artificial neural networks. J Membr Sci 2003;217:69–86.
[53] Liu QF, Kim SH, Lee S. Prediction of microfiltration membrane fouling using artificial neural network models. Sep Purif Technol 2009;70:96–102.
[54] Liu QF, Kim SH. Evaluation of membrane fouling models based on bench-scale experiments: a comparison between constant flow rate blocking laws and artificial neural network (ANNs) model. J Membr Sci 2008;310:393–401.
[55] Curcio S, Calabrò V, Iorio G. Reduction and control of flux decline in cross-flow membrane processes modeled by artificial neural networks. J Membr Sci 2006;286:125–132.
[56] Aydiner C, Demir I, Yildiz E. Modeling of flux decline in crossflow microfiltration using neural networks: the case of phosphate removal. J Membr Sci 2005;248:53–62.
[57] Chew CM, Aroua MK, Hussain MA. A practical hybrid modeling approach for the prediction of potential fouling parameters in ultrafiltration membrane water treatment plant. J Ind Eng Chem 2017;45:145–155.
[58] Ren J, Wang R. Preparation of polymeric membranes. In: Wang LK, Chen JP, Hung Y-T, Shammas, editors. Volume 13 of the series handbook of environmental engineering – membrane and desalination technology. New York: Springer, 2010:47–100.
[59] Baker RW. Membrane technology and applications. New York: McGraw-Hill, 2000.
[60] Reuvers AJ, Van den Berg JW, Smolders CA. Formation of membranes by means of immersion precipitation: part I. A model to describe mass transfer during immersion precipitation. J Membr Sci 1987;34:45–65.
[61] Akthakul A, Scott CE, Mayes AM, Wagner AJ. Lattice Boltzmann simulation of asymmetric membrane formation by immersion precipitation. J Membr Sci 2005;249:213–226.
[62] Yong SK, Hyo JK, Un JK. Asymmetric membrane formation via immersion precipitation method I. Kinetic effect. J Membr Sci 1991;60:219–232.
[63] Pereira CC, Nobrega R, Borges CP. Spinning process variables and polymer solution effects in the die-swell phenomenon during hollow fiber membranes formation. Brazilian J Chem Eng 2000;17:4–7.
[64] Di Luccio M, Nobrega R, Borges CP. Microporous anisotropic phase inversion membranes from bisphenol-A polycarbonate: study of a ternary system. Polymer 2000;41:4309–4315.
[65] van de Witte P, Dijkstra PJ, Van den Berg JW, Feijen J. Phase separation processes in polymer solutions in relation to membrane formation, J. Membr Sci 1996;117:1–31.
[66] Khulbe KC, Feng CY, Matsuura T. Membrane Characterization in Desalination and Water Resources Membrane Processes, vol. 1, ed. DMK Al-Gobaisi. Paris, France: EOLSS, 2010:131–172.
[67] Tung KL, Chang KS, Wu TT, Lin NJ, Lee KR, Lai JY. Recent advances in the characterization of membrane morphology. Curr Opin Chem Eng 2014;4:121–127.
[68] Tylkowski B, Tsibranska I. Overview of main techniques used for membrane characterization. J Chem Technol Metall 2015;50:3–12.
[69] Hernández A, Calvo JI, Prádanos P, Tejerina F. Pore size distributions in microporous membranes. A critical analysis of the bubble point extended method. J Membr Sci 1996;112:1–12.
[70] Kaneko K. Determination of pore size and pore size distribution: 1. Adsorbents and catalysts. J Membr Sci 1994;96:59–89.
[71] Calvo JI, Hernadez A, Pradanos P, Martinez L, Bowen WR. Pore size distributions in microporous membranes II. Bulk characterization of track-etched filters by air porometry and mercury porosimetry. J Colloid Interface Sci 1995;176:467–478.
[72] Cao GZ, Meijerink J, Brinkman HW, Burggraaf AJ. Permporometry study on the size distribution of active pores in porous ceramic membranes. J Membr Sci 1993;83:221–235.

[73] Zhao C, Zhou X, Yue Y. Determination of pore size and pore size distribution on the surface of hollow-fiber filtration membranes: a review of methods. Desalination 2000;129:107–123.
[74] Glaves CL, Smith DM. Membrane pore structure analysis via NMR spin-lattice relaxation measurements. J Membr Sci 1989;46:167–184.
[75] Jeon JD, Kim SJ, Kwak SY. ^{1}H nuclear magnetic resonance (NMR) cryoporometry as a tool to determine the pore size distribution of ultrafiltration membranes. J Membr Sci 2008;309:233–238.
[76] Vanegas ME, Quijada R, Nunes SP, Yave W. Syndiotactic polypropylene copolymer membranes and their performance for oxygen separation. J Membr Sci 2010;348:34–40.
[77] Zhao CT, Rosário Ribeiro M, De Pinho MN, Subrahmanyam VS, Gil CL, De Lima AP. Structural characteristics and gas permeation properties of polynorbornenes with retained bicyclic structure. Polymer 2001;42:2455–2462.
[78] Recio R, Palacio L, Prádanos P, Hernández A, Lozano AE, Marcos A, et al. Gas separation of 6FDA–6FpDA membranes. Effect of the solvent on polymer surfaces and permselectivity. J Membr Sci 2007;293:22–28.
[79] Baker EA, Rittigstein P, Torkelson JM, Roth CB. Streamlined ellipsometry procedure for characterizing physical aging rates of thin polymer films. J Polym Sci B 2009;47:2509–2519.
[80] Xu Z, Huang X, Wan L. Surface Engineering of Polymer Membranes. Hangzhou, China ang Berlin, Germany: Zhejiang University Press and Springer; 2009.
[81] Ho WS, Sirkar KK, editors. Membrane handbook. New York: Van Nostrand Reinhold, 1992.
[82] Quinson JF, Mameri N, Guihard L, Bariou B. The study of the swelling of an ultrafiltration membrane under the influence of solvents by thermoporometry and measurement of permeability. J Membr Sci 1991;58:191–200.
[83] Colby AH, Colson YL, Grinstaff MW. Microscopy and tunable resistive pulse sensing characterization of the swelling of pHresponsive, polymeric expansile nanoparticles. Nanoscale 2013;5:3496–3504.
[84] Ogieglo W, Werf H, Tempelman K, Wormeester H, Wessling M, Nijmeijer A, et al. n-Hexane induced swelling of thin PDMS films under non-equilibrium nanofiltration permeation conditions, resolved by spectroscopic ellipsometry. J Membr Sci 2013;437:313–323.
[85] Mele A, Castiglione F, Malpezzi L, Ganazzoli F, Raffaini G, Trotta F, et al. HR. MAS, NMR, powder XRD and Raman spectroscopy study of inclusion phenomena in CD nanosponges. J Incl Phenom Macrocycl Chem 2011;69:403–409.
[86] Diaper C, Correia V, Judd S. Characterisation of zirconium/poly(acrylic acid) low pressure dynamically formed membranes by use of the extended Nernst-Planck equation. J Membr Sci 1998;138:135–140.
[87] Hassan AR, Ali N, Abdull N, Ismail AF. A theoretical approach on membrane characterization: the deduction of fine structural details of asymmetric nanofiltration membranes. Desalination 2007;206:107–126.
[88] Tompa H. Polymer solutions. London: Butterworths Scientific Publications; 1956.
[89] Altena FW, Smolders CA. Calculation of liquid-liquid phase separation in a ternary system of a polymer in a mixture of a solvent and a nonsolvent. Macromolecules 1982;15:1491–1497.
[90] Tsay CS, McHugh AJ. Mass transfer modeling of asymmetric membrane formation by phase inversion. J Polym Sci Polym Phys Ed 1990;28:1327–1365.
[91] Cohen C, Tanny GB, Prager S. Diffusion-controlled formation of porous structures in ternary polymer system. J Polym Sci Polym Phys Ed 1979;17:477–489.
[92] Reuvers AJ, Van den Berg JW, Smolders CA. Formation of membranes by means of immersion precipitation. Part I. A model to describe mass transfer during immersion precipitation. J Membr Sci 1987;34:45–65.
[93] Kim YD, Kim JY, Lee HK, Kim SC. A new modeling of asymmetric membrane formation in rapid mass transfer system. J Membr Sci 2001;190:69–77.
[94] Wang XL, Qian JJ, Chen LJ, Lu ZY, Li ZS. Dissipative particle dynamics simulation on the polymer membrane formation by immersion precipitation. J Membr Sci 2008;311:251–258.
[95] Akthakul A, Scott CE, Mayes AM, Wagner AJ. Lattice–Boltzmann simulation of asymmetric membrane formation by immersion precipitation. J Membr Sci 2005;249:213–226.
[96] Zhou B, Powell AC. Phase field simulations of early stage structure formation during immersion precipitation of polymeric membranes in 2D and 3D. J Membr Sci 2006;268:150–164.
[97] He X, Chen C, Jiang Z, Su Y. Computer simulation of formation of polymeric ultrafiltration membrane via immersion precipitation. J Membr Sci 2011;371:108–116.
[98] Xu X, Cao D, Wu J. Density functional theory for predicting polymeric forces against surface fouling. Soft Matter 2010;6:4631–4646.